


RESEARCH

Open Access



Unveiling the potential of MSC extracellular vesicles: MiR-122-5p enhancing chondrocyte regeneration in osteoarthritis via autophagy mechanism

Haifeng Zhang^{1,2,3,4†}, Yanmeng Yang^{5†}, Yingnan Wu^{1,2}, Vinitha Denslin², Yi Wei Justin Koh¹, Ling Liu⁶, Wenhai Zhuo^{1,2}, Wing Moon Raymond Lam^{1,2}, Yinxian Yu^{3*}, James Hoi Po Hui^{1,2,7} and Zheng Yang^{1,2*} 

Abstract

Background Osteoarthritis (OA) is one of the most prevalent degenerative joint diseases, while the mechanism by which extracellular vesicles (EVs) promote chondrocyte regeneration remains unclear. The study assessed the effect of hypoxic mesenchymal stem cells (MSCs)-derived EVs on cartilage repair in a rat OA model.

Methods The effects of EVs on chondrocyte regeneration and autophagy were evaluated in vitro. The influence of specific micro RNA (miRNA) and downstream target genes was examined following EV miRNA sequencing and multiple intersecting database analysis.

Results We found EVs derived from hypoxia preconditioned human MSCs to promote cartilage repair in rat OA and enhance the proliferation and migration of chondrocytes in vitro, mediated via chondrocyte autophagy. MiRNA sequencing revealed a significant enrichment of miRNA122-5p in hypoxic MSCs EV, which through regulation of the target gene, *DUSP2*, mediated autophagy and participated in chondrocyte regeneration. *DUSP2* regulation of chondrocyte autophagy could act via the phosphorylation of ERK1/2 and P38.

Conclusions This study demonstrates that EVs released by MSCs under hypoxic conditions have a beneficial effect on chondrocyte regeneration. A novel mechanism for chondrocyte autophagy is mediated by miR122-5P and *DUSP2* target molecules, providing new insights into OA treatments.

Keywords Osteoarthritis, Chondrocyte, Extracellular vesicles, Autophagy, miR-122-5p, *DUSP2*

[†]Haifeng Zhang and Yanmeng Yang are co-first authors.

*Correspondence:

Yinxian Yu
eastpool@sjtu.edu.cn
Zheng Yang
dosyz@nus.edu.sg

¹Department of Orthopedic Surgery, Yong Loo Lin School of Medicine, National University of Singapore, Singapore, Singapore

²NUS Tissue Engineering Program, Life Sciences Institute, National University of Singapore, 27 Medical Drive, DSO (Kent Ridge) Building, level 4, Singapore 117510, Singapore

³Department of Orthopaedic Surgery, Shanghai General Hospital, Shanghai Jiao Tong University School of Medicine, Shanghai 200080, China

⁴Department of Orthopaedic Surgery, the First Affiliated Hospital of Soochow University, Suzhou City, China

⁵Critical Analytics for Manufacturing Personalised-Medicine, Singapore-MIT Alliance for Research and Technology, Singapore, Singapore

⁶Research Office, Sengkang General Hospital, Singapore, Singapore

⁷Department of Orthopedic Surgery, National University Hospital, Singapore, Singapore



© The Author(s) 2025. **Open Access** This article is licensed under a Creative Commons Attribution-NonCommercial-NoDerivatives 4.0 International License, which permits any non-commercial use, sharing, distribution and reproduction in any medium or format, as long as you give appropriate credit to the original author(s) and the source, provide a link to the Creative Commons licence, and indicate if you modified the licensed material. You do not have permission under this licence to share adapted material derived from this article or parts of it. The images or other third party material in this article are included in the article's Creative Commons licence, unless indicated otherwise in a credit line to the material. If material is not included in the article's Creative Commons licence and your intended use is not permitted by statutory regulation or exceeds the permitted use, you will need to obtain permission directly from the copyright holder. To view a copy of this licence, visit <http://creativecommons.org/licenses/by-nc-nd/4.0/>.

Background

Osteoarthritis (OA) is a common joint disease that mainly affects the elderly population [1]. The pathological changes in OA manifest as whole joint lesions, mainly involving the articular cartilage, subchondral bone, synovium, ligaments, and meniscus [2]. The etiology of OA is multifactorial, including factors like obesity, aging, genetics, and inflammation factors [3]. A major contributor to cartilage lesions in OA is the increase in inflammatory cytokines such as IL-1 β [4]. Currently, the treatment methods for OA are based on a stepwise approach, such as anti-inflammatory drug therapy and reconstructive surgery, depending on the severity level of the disease [5].

Autophagy has been implicated in the pathogenesis of OA [6], with results suggesting that autophagy activation reduces the severity of OA, possibly by the promotion of extracellular matrix homeostasis of chondrocytes, but the underlying mechanisms of autophagy on the pathological progression of OA are still largely unknown [7, 8]. When faced with adverse external stresses, such as nutrient deficiency and redox stress, cells could maintain homeostasis by digesting their own substances in a process termed autophagy [9]. The dynamic process of autophagy involves multiple steps, including the induction of phagophore, elongation, maturation, and degradation of the autophagosome [10]. Many autophagy-related genes participate in cellular catabolic processes, while abnormal autophagy is implicated in physiological and pathological conditions. Regulation of autophagy thus offers the potential in ameliorating various diseases [11].

Due to their ability to self-renew and differentiate, mesenchymal stem cells (MSCs) have been demonstrated as promising cell sources for tissue regeneration [12]. Furthermore, MSCs exert extensive paracrine effects via secreted extracellular vesicles (EVs), playing critical roles in regulating a variety of diseases [12]. Recent studies have shown that intra-articular injection of stem cell-derived exosomes elicited promising results in cartilage repair, which were attributed to the proteins, miRNAs and lipids packaged within the EVs [13]. The therapeutic efficacy of MSCs EVs in cartilage repair has been associated with EV-mediated autophagy regulation for the control of disease progression [14–16].

Hypoxia preconditioned was demonstrated to significantly enhance MSCs paracrine activities [17–19]. EVs extracted from hypoxic-MSCs (H-EVs) were shown to have increased chondrogenic, chemotactic, proliferative, anti-inflammatory and anti-apoptotic properties [17, 19]. When delivered to the intra-articular rat joint with osteochondral defect, H-EVs efficiently promoted bone and cartilage regeneration and inhibit synovial inflammation [17]. In this study, the therapeutic effect of MSC derived H-EV was validated in a rat OA model. The mechanism-of-action of EVs was investigated, in particular, EVs'

regulation in autophagy, and the alteration of autophagy levels on the regeneration of chondrocytes. Highly expressed miR-122-5p was screened out by miRNA sequencing in H-EVs and the effect and mechanism-of-action of miR-122-5p on chondrocyte regeneration was studied.

Methods

Reagents and antibodies

Recombinant Human IL-1 beta/IL-1F2 Protein was purchased from the R&D systems (201-LB, Minneapolis, USA). Rapamycin (RAPA, HY-10219, autophagy activator), salubrinal (HY-15486, DUSP2 inhibitor) were obtained from MedChemExpress company (MCE, New Jersey, USA). Protease inhibitor (A32955) and phosphatase inhibitor (78420) were from Thermo Scientific. Primary antibodies used in Western blotting are as follows: Exosome Panel, including CD9, CD63, and CD81 (1:1000, ab275018, Abcam), anti-LC3B (1:1000, ab48394, Abcam), anti-SQSTM1/p62 (1:1000, ab91526, Abcam), anti-DUSP2 (1:500, sc-32776, Santa Cruz), anti-HIF1 α (1:500, sc-53546, Santa Cruz), anti-p38 MAPK (1:1000, #9212, CST), anti-p44/42 MAPK (Erk1/2) (1:1000, #4695, CST), anti-p44/42 MAPK (Erk1/2) (phospho Thr202/Tyr204) (1:1000, ab214362, Abcam), anti-p38 (phospho T180 + Y182) (1:1000, ab4822, Abcam), anti-beta actin (1:1000, ab6276, Abcam), anti-GAPDH (1:1000, ab8245, Abcam), anti-MMP13 (1:1000, ab39012, Abcam), anti-type I collagen, (1:1000, C2456, Sigma-Aldrich), anti-type II collagen antibody (1:1000, MAB8887, Sigma-Aldrich), anti-aggrecan (1:1000, MA3-16888, Invitrogen). Secondary antibodies are used as follows: HRP-conjugated goat anti-rabbit, goat anti-mouse antibodies were purchased from Abcam Company. Goat anti-rabbit IgG H&L (Alexa Fluor[®] 488, ab150077, Abcam), goat anti-mouse IgG H&L (Alexa Fluor[®] 647, ab150115, Abcam), goat anti-mouse IgG1 cross-adsorbed secondary antibody (Alexa Fluor[™] 488, # A-21121, Invitrogen), goat anti-rabbit IgG (H + L) cross-adsorbed secondary antibody (Alexa Fluor[™] 594, #A-11012, Invitrogen), Alexa Fluor[™] 488 Phalloidin (A12379, Invitrogen), TRITC-conjugated phalloidin and DAPI (Merck, FAK100).

Bioinformatics analysis

The GEO Database (<https://www.ncbi.nlm.nih.gov/geo/>) and functional genomics database ArrayExpress (<https://www.ebi.ac.uk/biostudies/arrayexpress>) were selected to search and screen high throughput sequencing datasets with the key word “osteoarthritis” or “OA” and “RNA-Sequence” or “RNA-Seq” within the organism of *Homo sapiens* for the bulk RNA analysis. We also selected the GEO database with the key word “osteoarthritis” or “OA” and “single cell” or “scRNA” within the organism of *Homo sapiens* for the single cell high throughput

sequencing analysis. Based on the filtering criteria, GSE114007 (38 samples), E-MTAB-6266 (70 samples), and E-MTAB-7313 (54 samples) were selected for the following analysis. The high-throughput datasets were from the following platforms: GPL11154: Illumina HiSeq 2000 (Homo sapiens), Illumina HiSeq 2500 platform (Homo sapiens), Illumina HiSeq 2000 System (Homo sapiens), separately.

To further evaluate the level of autophagy in osteoarthritis, we used open autophagy databases, including the THANATOS database (<http://thanatos.biocuckoo.org>), HADb (<http://www.autophagy.lu/index.html>), HAMdb (<http://hamdb.scbdd.com/>) and Autophagy Database (<http://autophagy.info/>), to collect human-related autophagy genes. By intersecting the autophagy-related genes with the differential expression genes from above bulk transcription databases in OA groups, we screened for the autophagy-related gene molecules in OA.

To predicted the down-stream target genes of miR-122-5P, five main miRNA databases, including TargetScanHuman8.0 (https://www.targetscan.org/vert_80/), miRPathDB 2.0 (<https://mpd.bioinf.uni-sb.de/>), RNA22 (<https://cm.jefferson.edu/rna22/>), and miRtarbase (<https://mirtarbase.cuhk.edu.cn/>) as well as a database of miRNA profiling in extracellular vesicles, EVmiRNA (<http://bioinfo.life.hust.edu.cn/EVmiRNA/>), were used to analyze and narrow down the range of target genes by intersection following default parameters. Finally, we selected an open source software platform, Cytoscape [20], for visualizing integrating networks and identify the downstream autophagy target genes of miR-122-5P in OA.

For the scRNA-seq analysis method, we downloaded and processed the GSE196678 dataset for each sample using the “Seurat” package (version 4.0; <http://satijalab.org/seurat/>) with R software (version 4.2). The high-throughput scRNA sequencing dataset was from the GPL24676 Illumina NovaSeq 6000 (Homo sapiens) platforms. The following filter conditions are set: $nFeature_RNA > 400$ & $nFeature_RNA < 3000$ & $percent.mt < 15$ & $nCount_RNA > 1500$ & $nCount_RNA < 10,000$. `NormalizeData` function was used to normalize all the data, and `FindVariableFeatures` function was used to filter highly variable genes (HVGs), where $nfeatures = 4000$. `ScaleData` function was used to normalize HVGs and perform PCA dimensionality reduction, visualize on two-dimensional maps by the tSNE function after clustering cells using the `FindClusters` function. Then, we selected the SingleR annotation cell type. Finally, DEG was determined with $\logFCfilter = 0.5$ and $adjPvalFilter = 0.05$ as the differential gene screening criteria.

We select the R language analysis package (R 4.2.2) to analyze all the genesets, using the `limma` function to calculate the differential expression genes, `pheatmap`

packages to visualize heat maps, the `ggplot2` function to draw volcanic maps, the `EnrichGO` and `EnrichKEGG` packages in the `GOplot` function to complete functional enrichment analysis. At the same time, we selected the open database, String website (<https://string-db.org>), an authoritative protein-protein interaction network to predict of the target genetic regulatory molecular.

Human bone marrow MSCs culture

Human bone marrow MSCs were purchased from Lonza Inc. (Walkersville, MD, USA) and provided in passage 2. MSCs were cultured in 1 g/L d-Glucose Dulbecco's Modified Eagle's Medium (DMEM, Gibco) supplemented with 10% fetal bovine serum (FBS) (Hyclone, Logan, UT, USA), 1% Penicillin-Streptomycin (P/S, Life Technologies, USA) and 1% GlutaMAX (Thermo Fisher Scientific). All experiments used cells in 4–5 passages.

Human chondrocytes culture

Chondrocytes derived from human were acquired from Innoprot Inc. (P10970, Derio, Spain). Chondrocytes were cultured in DMEM supplemented with 10% FBS and 1% GlutaMAX, and 1% P/S. Cells at passage 2 were used for all experiments.

For chondrocyte re-differentiation, chondrocytes (2×10^5) suspended in chondrogenic media were centrifuged at 200 g for 5 minutes to form pellets and cultured in chondrogenic media containing 5 ng/mL TGF- β 3 (RnD Systems, Canada) [17]. To induce inflammation, 5 ng/ml IL-1 β was included in the chondrogenic medium. EVs at 1x concentration and different autophagy intervention reagents were supplemented accordingly.

OA chondrocytes were extracted from femoral condyles of discarded knee tissues of total knee replacement patients ($n = 5$). Consent for using patient tissue was according to the guidelines of National Healthcare Group Domain Specific Review Board (NHG DSRB Ref: 2024–3392). Briefly, cartilage excised from the discarded knee was diced and digested at 37 °C in 0.25% (w/v) type-II collagenase overnight. Chondrocytes isolated were then subjected to PCR and western blot analysis.

293T/17 cell culture

293T/17 cells were obtained from ATCC (CRL-11268™) were supported by National University of Singapore Center of Cancer Research. Cells were cultured in DMEM (Gibco, 11995–065) supplemented with 1% P/S and 10% FBS. Cells were maintained in a humidified incubator at 37 °C, 5% CO₂.

Hypoxia preconditioning of MSC and EVs isolation

MSCs were cultured under 1% or 20% oxygen tension for 24 h in serum-free DMEM to collect hypoxia and normoxia conditioned medium. The collected conditioned

medium was centrifuged at 500 g for 5 min, followed with 4000 g for 10 min to remove cell debris. Cell numbers were counted after conditioned medium collection and used for normalization. The conditioned medium was concentrated 10 times using protein concentrators with a molecular weight cut-off of 30 kDa (Thermo Fisher Scientific, USA). EVs were collected using size-exclusion chromatography on a q-EV2 column (Izon, New Zealand) according to the manufacturer's instructions. EVs were diluted to niche (1x) concentration and used in EV characterization and the in vitro functional assays.

Protein concentrations of EVs were measured with a Micro BCA Protein Assay Kit (ThermoFisher, USA). Nanoparticle tracking analysis (NTA) was performed on NanoSight NS500 instrument (NanoSight Ltd, UK) to determine the particle size and numbers of EVs. The morphology of EVs was imaged by transmission electron microscopy (TEM; JEOL JEM-1220).

Visualization of EVs internalization within chondrocytes

EVs were labeled with PKH67 green fluorescent cell linker according to manufacturer's protocol (Sigma-Aldrich, MINI67-1KT). EVs solution was concentrated and purified to remove excess PKH67 as described above. PKH67-labeled EVs were co-cultured with chondrocytes for 8 h. Uptake of EVs evaluated by Nikon Ti2-E fluorescence microscopy.

OA model in vivo

Eighteen healthy female Sprague Dawley rats (8 weeks old) with a weight range of 220–250 g were provided by the Experimental Animal Center of National University of Singapore. All animal procedures were performed according to the guidelines of the Institutional Animal Care and Use Committee at National University of Singapore (IACUC protocol number: R2020-0258). The work has been reported in line with the ARRIVE guidelines 2.0. Before operation, the animals were treated to isoflurane anaesthesia in an induction chamber in which the oxygen flow was set at 1 L/min vaporizer adjusted to 3%. The OA model was induced by anterior cruciate ligament transection (ACLT) on the right knee. The left knee served as a sham group underwent the same procedure, with the anterior cruciate ligament remaining intact. Four weeks post-operation, the ACLT knees were randomly allocated and subjected to multiple weekly injection for 6 weeks with EVs from normoxia MSCs (N-EVs; $n=6$) or hypoxia MSC (H-EVs; $n=6$) containing 120 μg of total EVs protein in 100 μL of PBS. ACLT knee injected with equivalent volume of PBS served as the control ($n=6$). The sample size was decided based on power calculation from the website: <https://clincalc.com/stats/samplesize.aspx>; continuous end point, two independent sample study.

Animals were kept 2 per cage at a temperature of 20–24°C, humidity of 50–60%, and a 12/12-hour light/dark cycle. Pain killer, ibuprofen (40 mg/ml, 20 mg/kg), was provided for 3 days post-operation and antibiotic, Enrofloxacin (100 mg/ml, 15 mg/kg) was provided for 5 days by Subcutaneous injection once per day. The animals were monitored for 7 days. Post-op rat pain observations include changes in normal activity levels, such as reduced movement or reluctance to explore, as well as signs of discomfort like vocalizations, grooming of the surgical site, or abnormal postures. Animals were excluded based on significant weight loss (more than 10% of their body weight), general signs of pain or distress (such as lethargy, abnormal posture, or vocalization), or systemic infections (evidenced by fever, abnormal blood work, or visible signs of illness). In the case of humane endpoint, over dose Xylazine + ketamine would be administered after the animals were sedated by Isoflurane.

Micro-CT analysis

To evaluate morphological features of bone tissue around the knee joint, rat knee joints sample were first fixed in 10% formalin (Sigma-Aldrich, MO, USA). The samples were subsequently scanned by Quantum FX μCT system (PerkinElmer, Waltham, MA, USA). The scanning parameters were set as follows: Voltage 90 kV, Current 160 μA , FOV, axial 10 mm, Voxel size 20 μm . The regions of interest (ROIs) at the subchondral bone trabecular area were selected to collect data. 3D image reconstruction were performed using CTAn and the Mimics Medical 21.0 (Materialise NV) software, and trabecular bone microstructure was quantitatively analyzed, including bone volume over total volume (BV/TV), trabecular thickness (Tb.Th), trabecular number (Tb.N), bone mineral density (BMD), and the total volume of osteophytes.

Histological and immunological staining

To observe the histopathological changes in the knee joint, the samples were fixed in 10% formalin, decalcified with 10% EDTA solution, dehydrated, embedded, and sectioned into 6 μm slices. Tissue sections were subjected to hematoxylin and eosin (H&E) staining and safranin O staining. The osteoarthritis research society international (OARSI) grading was performed to assess the degree of joint degeneration [21].

For immunohistochemical and immunofluorescence staining, paraffin sections underwent routine dewaxing, hydration, pepsin retrieval, followed by UV blocking, incubation with primary and secondary antibodies, then DAB staining and hematoxylin counterstaining. All sections were imaged using Nikon Ti2-E microscope (Nikon, Tokyo, Japan) and images were analyzed using Image J software.

Quantitative real-time polymerase chain reaction (RT-qPCR)

RNAs were extracted with RNeasy® Mini Kit (Qiagen, Germany). Reverse transcription was conducted with 100 ng of total RNA using iScript™ cDNA synthesis kit (Bio-Rad, USA). Real-time PCR was performed using the Power SYBR® green PCR master mix on ABI Step One plus Real-time PCR System (Applied Biosystems, Life Technologies, USA). The expression levels of targeted genes were normalized to the reference gene GAPDH and were then calculated using the $2^{-\Delta\Delta C_t}$ formula with reference. All primer sequences were listed in Supplementary Table 1 A).

Western-blot assay

Cells were lysed with protease and phosphatase inhibitors to extract proteins, and the protein concentration was determined using Pierce™ BCA Protein Assay Kits (Thermo Scientific, NH, USA). Protein samples (20 µg) were electrophoretically separated on 6–12% SDS-PAGE gel. The proteins were subsequently transferred on methanol-activated PVDF membrane (Millipore), blocked with 5% BSA, treated by the primary antibody and specific species HRP-labeled secondary antibody. Protein bands were visualized on a gel imaging system (Biorad) using the Pierce ECL Western Blotting Substrate (Thermo Scientific) and analyzed with Image J software.

Cell proliferation

Cell Counting Kit-8 (CCK-8) assay (Dojindo Molecular Technologies Inc.) was used to determine cell growth and proliferation of chondrocytes. 5×10^3 cells per well were cultured in 96-well plate and treated with gradient concentrations of reagents before incubation with CCK8 reagent for 2 h. The OD value was recorded by a microplate reader (Infinite M Nano + from Tecan) at 450 nm.

The proliferation of chondrocytes was also assessed by Ki-67 immunofluorescence and quantification of proliferative cells was evaluated by ImageJ software.

Cell migration

The migration effect of EVs originated from MSCs on chondrocytes was assessed using a culture (Millipore, Germany) and cell scratch test. For transwell assay, chondrocytes (5×10^4) were suspended in 300 µl of 0.5% FBS culture medium and placed into the upper chamber of 8.0-µm pore size mesh separating the upper and lower chambers in 24-well plates. The EVs were diluted in 0.5% FBS culture medium and added in 700 µl to the lower chamber of the transwell culture. After 24 h incubation, the migrated cells were fixed in 4% paraformaldehyde and stained with 0.1% crystal violet (Sigma Aldrich) for 20 min.

For the cell scratch test, chondrocytes (1×10^5 per well) were seeded in 6-well plates overnight and a vertical scratch was introduced before EVs and different intervention reagents were added for 24 h. Cell images were taken using an inverted microscope and the cell migration level were determined using ImageJ software.

MiRNA sequencing

RNAs were extracted from EVs using q-EV RNA extraction kit column (Izon, New Zealand). The sRNA library preparation and sequencing analysis was performed by Novogene (Singapore) with Illumina NextSeq 500 system. MiRNA expression levels were estimated by TPM (transcript per million): Normalized expression = mapped reads*1,000,000 (Supplementary Table 2). *P*-value of 0.05 was set as the threshold for significantly differential expression by default.

Vector plasmid construct and cell transfection

According to the sequence of DUSP2 3'UTR and hsa-miR-122-5p, the TargetScan database [18] (version:8.0) was used to predict the possible binding sites. GP-miR-GLO vector was used to construct DUSP2 WT-hsa-miR-122-5p and DUSP2 MUT-hsa-miR-122-5p plasmids, and designed miR-122-5p mimics and inhibitor, according to the manufacturer protocol (Genepharma, China). 293T cells transfection was performed using Lipofectamine® 2000 (Thermo Fisher) transfection solution in Opti-MEM™ (Thermo Fisher). All sequences are listed in Supplementary Table 1B.

Luciferase assay

The miR-122-5P mimics and EVs were added to human chondrocytes, followed by transfection with DUSP2-3'-UTR plasmid (Genepharma, China). Luciferase assays were performed with the Dual-Luciferase® Reporter Assay System (E1910, Promega Company). Normalization was calculated by co-transfection with Renilla plasmid. Determination of fluorescence value was recorded by Infinite M200 machine.

Statistical analysis

All survived animals were included for the data collection and statistical calculation. All statistical data were conducted by GraphPad Prism 8 software (GraphPad Software Inc., La Jolla, CA) and the outcomes were showed as means ± standard deviations. Both independent samples are normally distributed. Student's *t*-tests or Wilcoxon rank test were performed. Data from multiple groups that satisfy the homogeneity of variance, one-way ANOVA analysis was evaluated. Otherwise Kruskal Wallis test was used. A *P* value of less than 0.05 was considered statistically significant.

Results

Characterisation of EVs derived from MSCs

Human MSCs cultured under normoxia and hypoxia condition for 24 h showed similar cell morphology and proliferation (Fig. 1A). Western blot analysis showed that the hypoxia factor HIF-1 α was highly expressed by MSCs under hypoxic conditions (Fig. 1B). The shape and size of the isolated EVs was detected by TEM (Fig. 1C). NTA revealed similar EVs size distribution in both groups (Fig. 1D), with higher levels of EVs particles in hypoxia EVs (H-EVs). Western blot analysis showed higher expression of EVs marker CD63, CD81 and CD9, absence of EVs negative marker Calnexin (Fig. 1E), and BCA analysis suggested higher levels of EVs protein in the hypoxia group (Fig. 1F), indicating that hypoxia precondition promotes EVs production.

EVs promote chondrocyte regeneration in OA

In vivo efficacy of EV treatment was investigated using a rat ACLT OA model. No abnormal observation was found with the animal post-operation. All operated animals were included in the analysis. As shown in Supplementary Fig. 1A, H&E staining revealed that OA was well developed 8 weeks after ACLT. At 4 weeks after ACLT, EVs generated under normoxic and hypoxic conditions were injected into the knee joint weekly for 6

weeks (Fig. 2A). The micro-CT analysis suggested there were more osteophytes in OA groups and the number and volume of osteophytes decreased after EVs injection especially in hypoxia group (Fig. 2B, C). Quantitative analysis at the subchondral bone area revealed significant decreased proportion of BV/TV, Tb.Th and osteophyte volume, and increased Tb.N after EV treatments, with H-EVs treatment exerting significantly greater effect relative to N-EVs treatment (Fig. 2C), indicating that H-EVs treatment was more efficacious in ameliorating subchondral bone osteosclerosis. H&E staining revealed the unevenness of the cartilage articular surface, and bone cysts formation (circular vacuole structure) in some knee joints formation in the control OA group. EVs intervention improved integrity of articular surfaces (Fig. 2D). Safranin O staining suggested increased proteoglycan content in H-EVs group relative to the N-EVs group (Fig. 2E). IHC staining showed significant improvement of hyaline cartilage matrix COL2 and ACAN levels and the decreased level of COL1 in the H-EVs treatment group compared to the N-EVs group (Supplementary Fig. 1B, C). Overall suppression of OA progression was reflected in the OARSI score demonstrating significant improvement with H-EVs treatment (Fig. 2F).

To further investigate EVs function, in vitro studies were performed on human cartilage-derived

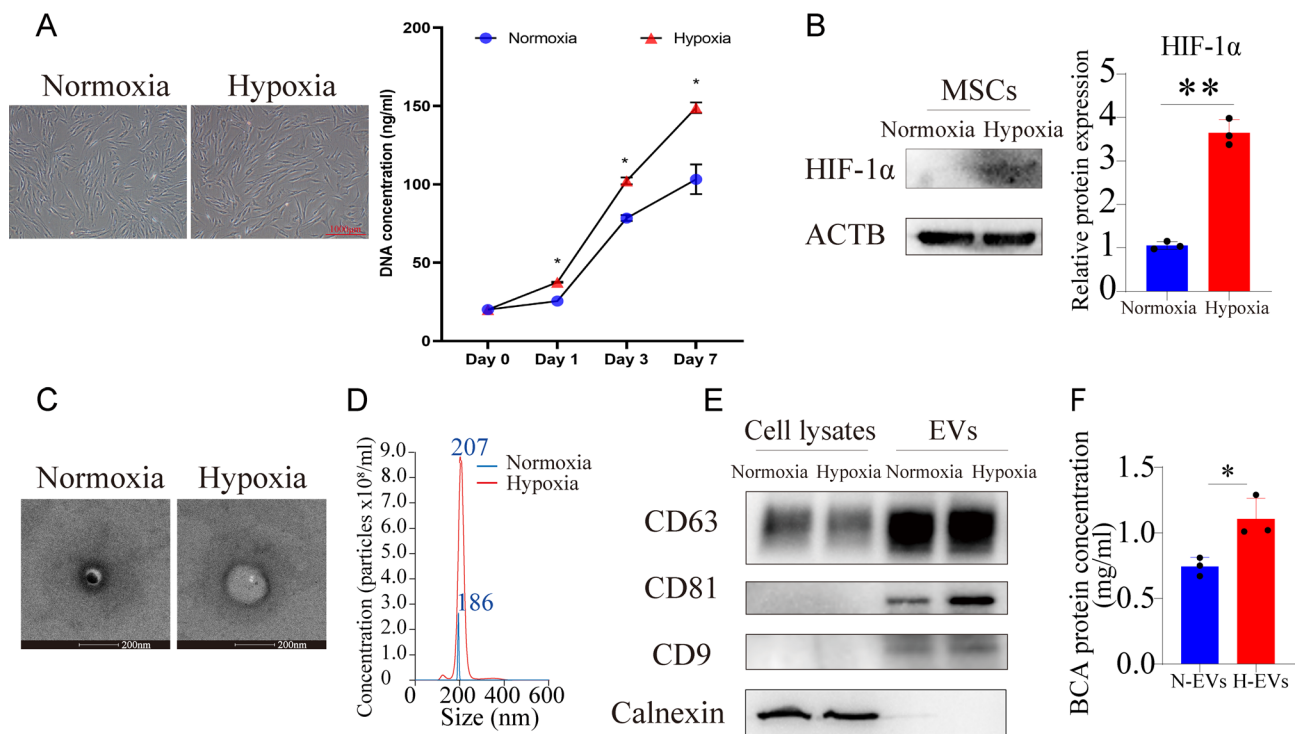


Fig. 1 Characterisation of normoxia and hypoxia MSC-derived EVs. **(A)** Growth state of MSCs under normoxic and hypoxic conditions. **(B)** Western blot analysis of HIF-1 α expression in MSCs. **(C)** Transmission electron microscopy (TEM) detection of isolated EVs. **(D)** Nanoparticle Tracking Analysis (NTA) of particle number and size analysis of HEV and NEV. **(E)** Expression of CD63, CD81, CD9 and Calnexin on EVs and cell lysate. **(F)** Comparison of protein concentration on EVs of MSCs in normoxic and hypoxic conditions. Full-length blots are presented in Supplementary Fig. 7

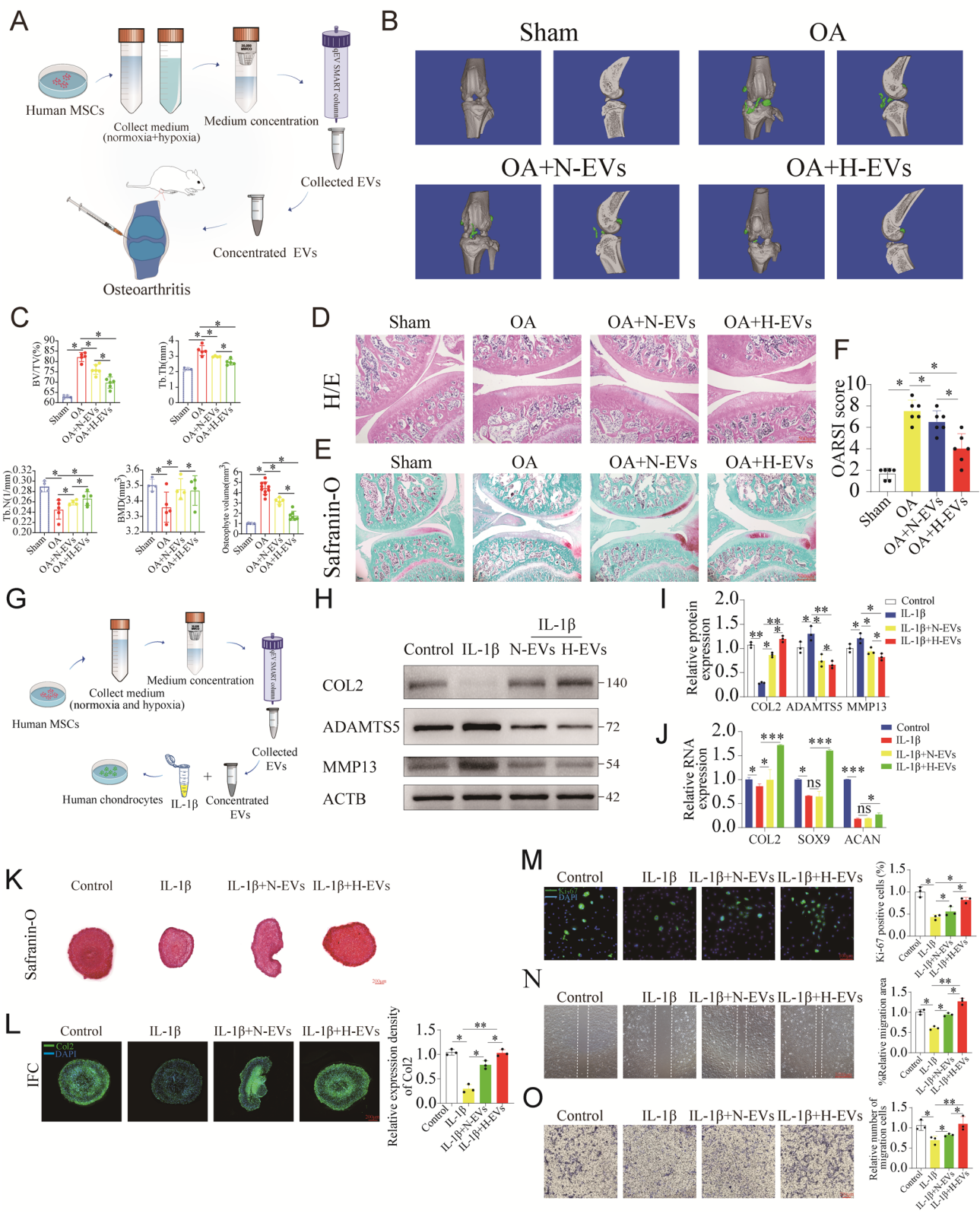


Fig. 2 (See legend on next page.)

(See figure on previous page.)

Fig. 2 The therapeutic effect of EVs on rat OA model and in vitro inflammatory-induced chondrocytes. **(A)** The flow chart of EVs generation from MSCs and injection to OA knees in rats. **(B)** Anterior and coronal views of microCT three-dimensional reconstruction of knee joint. Osteophytes were showed as green color and the volumes were quantitatively assessed. **(C)** Quantitative analysis of BV/TV, Tb.Th, Tb.N, BMD and osteophyte volume. **(D)** H&E and **(E)** Safranin O staining of knee. **(F)** OARSI score for cartilage regeneration. **(G)** Experimental set up to study the regenerative effect of EVs on IL1 β -induced chondrocytes in vitro. **(H, I)** Western blotting analysis of COL2, ADAMTS5, and MMP13 expression across different treatment groups. Full-length blots are presented in Supplementary Fig. 7. **(J)** RT-qPCR gene analysis of chondrocyte markers, COL2, SOX9, and ACAN. **(K)** Safranin O staining of chondrocyte pellets. **(L)** Immunofluorescence staining of COL2 in cartilage pellets and quantitative analysis of fluorescence intensity. **(M)** Assessment of chondrocyte proliferation assay with Ki-67 immunofluorescence staining. **(N)** Cell scratch assay and relative area to assess the cell migration across different groups. **(O)** Trans-well migration of chondrocytes and quantitative analysis of cell migration. Quantitative data represent mean \pm standard deviation, $n=3$; * denotes $p<0.05$ and ** $p<0.01$ relative to control group

chondrocytes. Firstly, internalization test of EVs was performed to assess uptake by chondrocytes. PKH67-stained EVs were shown to enter the chondrocytes within 8 h of co-culture (Supplementary Fig. 2A). In vitro inflammation condition was induced in chondrocytes using 5 ng/ml of IL-1 β in the presence or absence of EVs (Fig. 2G). Western blot and RT-qPCR analysis revealed significantly higher expression of COL2, SOX9 and ACAN, and the lower expression of ADAMTS5 and MMP13 in the H-EVs group compared to the IL-1 β group, and at enhanced level compared to N-EVs group (Fig. 2H-J). Higher expression of cartilage matrix formation under H-EVs treatment was further demonstrated in 3D cartilage pellet culture with increased safranin O and COL2 staining in the H-EVs group relative to other groups (Fig. 2K, L). Cell proliferation assay, as indicated by Ki-67 expression, suggested H-EVs significantly induced higher proliferative activity of chondrocytes (Fig. 2M). Migration studies with cell scratch assay and Trans-well migration assay found H-EVs significantly enhanced migration of chondrocytes in comparison to N-EVs (Fig. 2N, O).

EVs involved in the regulation of autophagy during chondrocyte regeneration

To investigate the autophagy effect during chondrocyte regeneration, Western blot analysis on chondrocytes cultured with IL-1 β at different times and concentrations were conducted. We found that the level of autophagy markers LC3I/II decreased while p62 increased when chondrocytes were subjected to 5ng/ml IL-1 β for 48 h, indicating IL-1 β induced autophagy suppression (Supplementary Fig. 3A-C).

Addition of both N-EVs and H-EVs increased the level of autophagy, with significantly higher effect by H-EVs as shown in Western blot and RT-qPCR analysis (Fig. 3A-C), and clearly demonstrated by IFC staining of the autophagy marker LC3 (Fig. 3D). TEM of chondrocytes suggests alteration in autophagosome number among different groups, with H-EVs treatment reversing IL-1 β induced effect (Fig. 3E). Co-staining of LC3 and cartilage matrix marker ACAN in rat OA knees suggested significantly higher expressions of LC3 and ACAN upon treatment with H-EVs relative to OA control group and N-EVs treatment group (Fig. 3F).

To confirm EVs regulation of autophagy during chondrocyte regeneration, EVs effect was investigated in the presence or absence of autophagy activators (rapamycin, RAPA, 10nM). The effective concentration of RAPA was determined by CCK8 test (Supplementary Fig. 2B). RAPA promotion of autophagy was demonstrated by RT-PCT, Western blot and IFC staining (Supplementary Fig. 4A-C, G), as well as change in autophagosome number (Supplementary Fig. 4D), and concurrently regeneration of chondrocytes. Inclusion of RAPA further promoted H-EVs effect on autophagy and chondrocyte regeneration including chondrocytes proliferation (Supplementary Fig. 4H) and migration (Supplementary Fig. 4I, J).

MiR-122-5p from EVs involved in the regulation of autophagy in chondrocytes

MiRNA-sequencing was performed on EVs from normoxic and hypoxic groups. 951 miRNAs were detected, of which the heatmap showed 50 abnormally expressed miRNAs between the two groups (Fig. 4A, Supplementary Table 2). Volcano map shown the 10 up-regulated miRNA and 5 down-regulated miRNA with false discovery rate (FDR) value greater than 1.5, including hsa-miR-19a-3p, hsa-miR-148-3p, and hsa-miR-122-5p (Fig. 4B). With miRNA-PCR identification, we found higher expression of hsa-miR-363-5p, hsa-miR-18a-5p, hsa-miR-122-5p, hsa-miR-126-5p, and hsa-miR-1260b, while hsa-miR-7f-1-3p with lower expression in the hypoxia group (Fig. 4C). As previous studies reported that hsa-miR-122-5p participated in the regulation of cell differentiation, metabolism and inflammation among these differentially expressed miRNAs [22, 23], hsa-miR-122-5p was selected for further investigation.

Figure 4D shows the secondary stem-loop structure of hsa-miR-122-5p for the generation of hsa-miR-122-5p mimics used in co-culture with IL-1 β treated chondrocytes. Western blot and RT-qPCR analysis showed the up-regulation of autophagy markers (Fig. 4E-H), increased autophagic vesicles (Fig. 4I), and higher expression of LC3 in IFC staining (Fig. 4J) under hsa-miR-122-5p mimic treatment. Inclusion of hsa-miR-122-5p mimics reverted the IL-1 β suppressed matrix formation (COL2 and ACAN) in chondrocytes while inhibiting the upregulation of degenerative markers (ADAMTS5 and

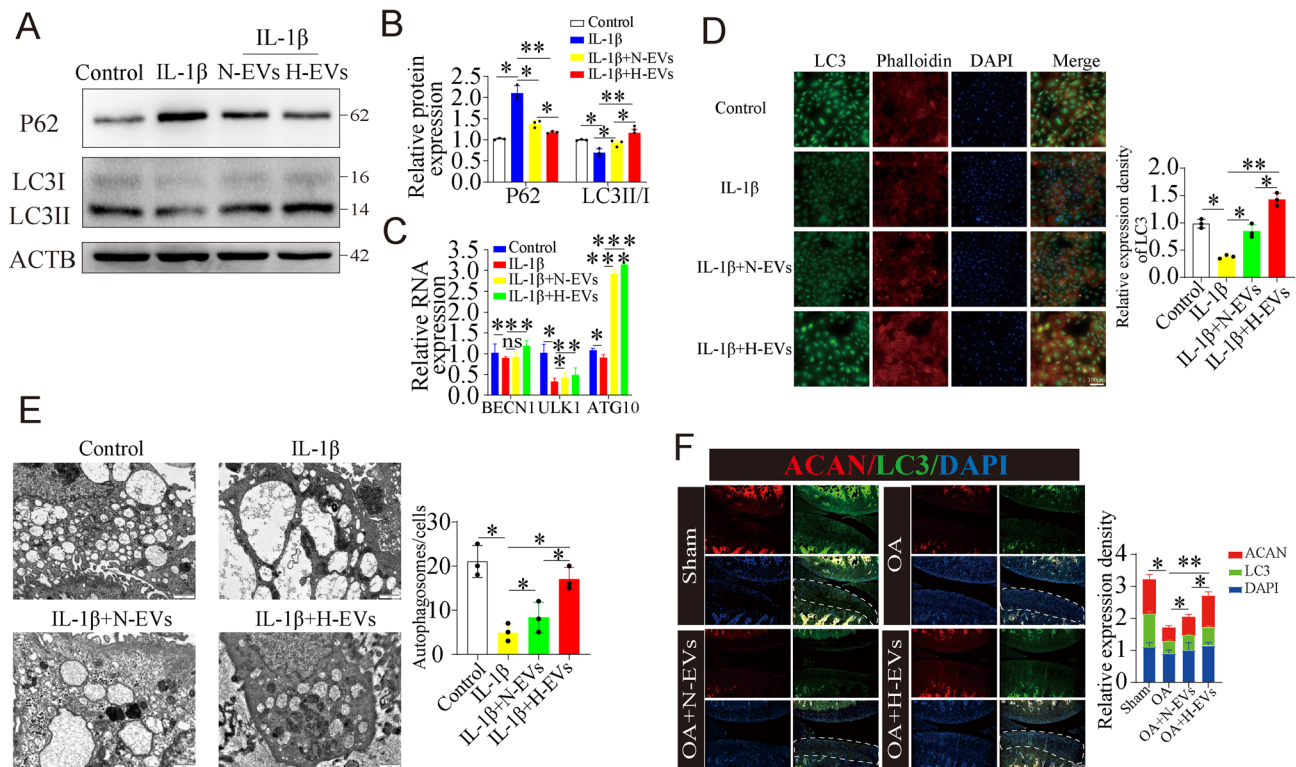


Fig. 3 Autophagy regulatory effect of EVs on chondrocytes. **(A, B)** Western blot analysis of autophagy proteins, P62 and LC3, expression. Full-length blots are presented in Supplementary Fig. 7. **(C)** RT-QPCR analysis on autophagy genes expression. **(D)** Immunofluorescence staining of LC3 in chondrocytes. **(E)** TEM images and quantitative analysis of autophagosomes. **(F)** Co-immunofluorescence staining of ACAN and LC3 on cartilage in OA knee. Quantitative data represent mean \pm standard deviation, $n=3$; * denotes $p < 0.05$ and ** $p < 0.01$ relative to control group

MMP13) as demonstrated by Western blot and RT-qPCR analysis (Fig. 4K, L). Staining of 3D-cultured cartilage pellets further demonstrate hsa-miR-122-5p mimics promotion of chondrocytes anabolic activity (Fig. 4M, N). Proliferation (Fig. 4O) and migration (Fig. 4P, Q) of chondrocytes were also enhanced with hsa-miR-122-5p mimics treatment.

Heighten expression of target gene DUSP2 in OA chondrocytes

To establish downstream target genes of hsa-miR-122-5p related to autophagy regulation, we acquired 1775 human autophagy-related genes from different main autophagy databases (Supplementary Fig. 5A and Supplementary Table 3). The acquired autophagy-related genes were then intersected with the human OA bulk-RNA sequence to further screen out 26 key molecules by Venn diagram (Supplementary Fig. 5B and Supplementary Table 4), including DAPK2, ZFP36 and DUSP2.

To predict the target genes of hsa-miR-122-5p, five main miRNA databases intersected into 36 target genes (Supplementary Fig. 5C and Supplementary Table 5). Finally, DUSP2 molecule was filtered out by Cytoscape software (Fig. 5A). In addition, single cell sequencing from OA samples were also further verified, the

differential gene were shown in Supplementary Tables 6, and 8 OA related cell clusters were enriched (Supplementary Fig. 5D). Focusing on chondrocytes, we analyzed the possible autophagy genes and found *DUSP2* genes to be abnormally expressed in OA chondrocytes, shown in bubble diagram (Supplementary Fig. 5E), and violin diagram (Fig. 5B).

IFC staining on rat OA samples found DUSP2 highly expressed in the nuclei of chondrocytes in the OA group compared to the sham group (Fig. 5C). In vitro, we also found higher expression of DUSP2 in chondrocytes under the stimulation of IL-1 β (Fig. 5D). The level of DUSP2 decreased after treatment with EVs both in vitro (Fig. 5D) and in vivo (Fig. 5C), and hsa-miR-122-5p mimic in vitro (Fig. 5E). Notably, lower expression of DUSP2 was observed in H-EVs treated group in both in vivo (Fig. 5C) and in vitro samples (Fig. 5F, G).

MiR-122-5P regulate the autophagy of chondrocytes by modulating DUSP2

To explore the possibility of miR-122-5p directly binding to DUSP2, TargetScan website was used to predict the miRNA-target interaction between DUSP2 3' UTR and hsa-miR-122-5p. As shown in Fig. 6A, we found potential binding sequence at the position 538–544 of DUSP2 3'

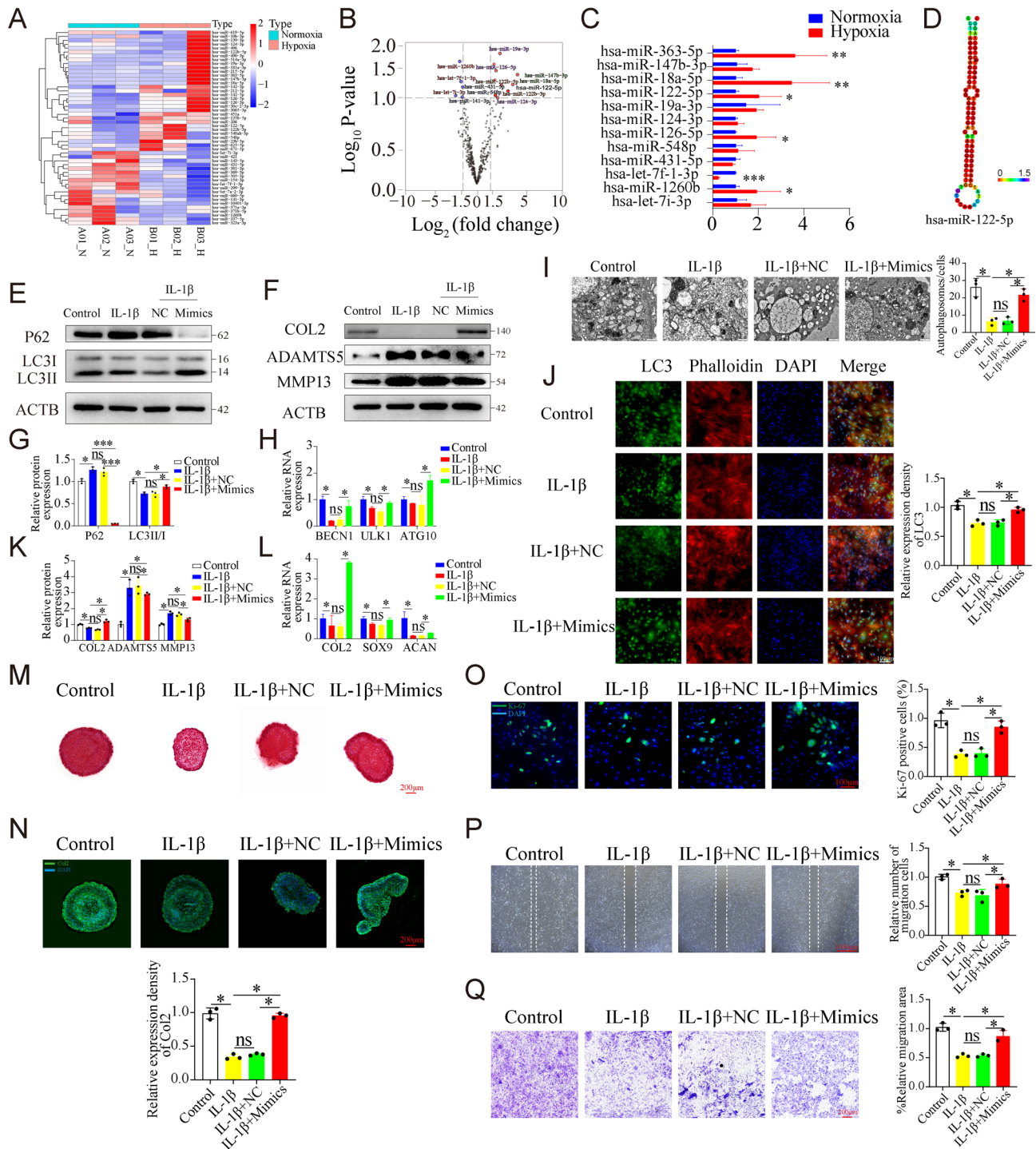


Fig. 4 miR-122-5p regulates chondrocyte autophagy. **(A)** Exosomal miRNA expression profile of MSCs under normoxic and hypoxic conditions. **(B)** Volcanic map of the differentially expressed miRNAs. **(C)** Real-time quantitative PCR verification of miRNAs expression. **(D)** The secondary stem ring structure of miR-122-5p. **(E, F)** Western blot analysis of autophagy protein, P62 and LC3, expression under hsa-miR-122-5p mimic (Mimics) treatment. NC = sham miRNA. **(G)** Expression of autophagy protein. **(H)** Expression of autophagy genes. **(I)** TEM analysis of autophagosomes. **(J)** Immunofluorescence staining and quantification of autophagy molecule LC3. **(K-L)** Regulation of chondrocytes expression matrix protein **(K)** and gene **(L)** expression by miR-122-5p. **(M)** Safranin O staining of chondrocyte pellets. **(N)** COL2 immunohistochemistry and quantification. **(O)** Ki-67 staining to analyse chondrocyte proliferation. **(P)** Cell scratch assay. **(Q)** Trans-well migration assay. ($n = 3$, mean \pm SD; * $p < 0.05$; ** $p < 0.01$; versus control group). Quantitative data represent mean \pm standard deviation, $n = 3$; * denotes $p < 0.05$ and ** $p < 0.01$ relative to control group. Full-length blots are presented in Supplementary Fig. 7

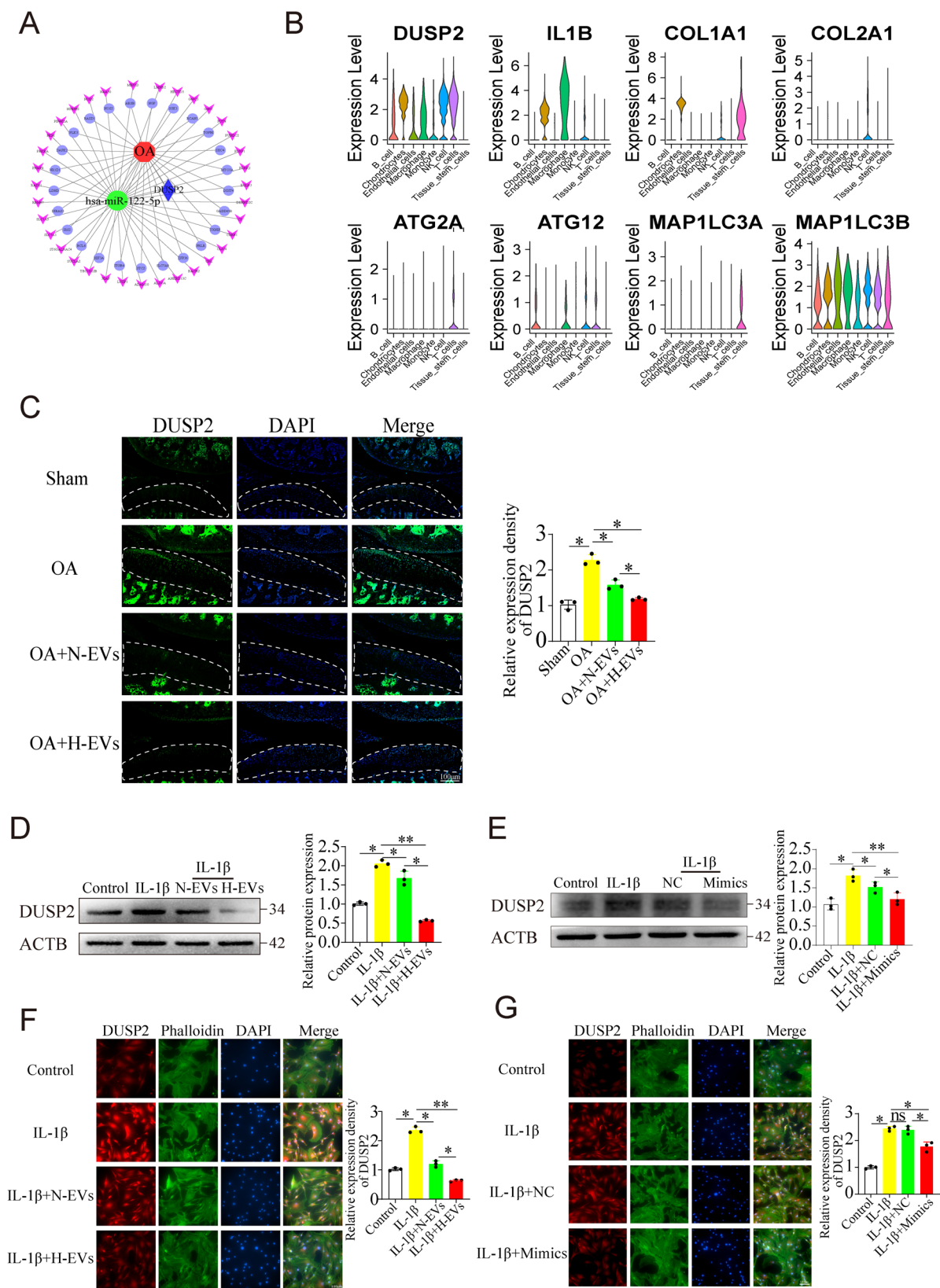


Fig. 5 (See legend on next page.)

(See figure on previous page.)

Fig. 5 Differential expression of DUSP2 in inflammatory chondrocytes. **(A)** Using Cytoscape software identification of potential downstream target genes regulated by miR-122-5p in OA. **(B)** Violin plot on the expression of autophagy-related genes, cartilage-related genes and DUSP2 in different cell types. **(C)** Immunofluorescence staining of DUSP2 in the cartilage layer after EVs treatment. **(D)** Western blot analysis on the expression of DUSP2 in IL-1 β -induced chondrocytes. **(E)** Expression of DUSP2 in chondrocytes under miR-122-5p mimics intervention. Immunofluorescence staining analysis of DUSP2 in chondrocytes under the intervention of IL-1 β and EVs **(F)** or miR-122-5p mimics **(G)**, Quantitative data represent mean \pm standard deviation, $n=3$; * denotes $p<0.05$ and ** $p<0.01$ relative to control group. Full-length blots are presented in Supplementary Fig. 7

UTR. The GFP-miRGLO plasmids synthesized according to these sequences were co-incubated with 293T cells. By performing luciferase assay, we found that fluorescence intensity was decreased in the wild-type but not in the mutant group after intervening by hsa-miR-122-5p mimics, indicating that there was a direct binding between hsa-miR-122-5p and DUSP2 3' UTR site (Fig. 6B). Luciferase assay also revealed reduced fluorescence intensity with N-EVs co-cultured 293T in the wild-type groups, and significantly lower fluorescence intensity with H-EVs treatment (Fig. 6B).

In order to validate that EVs regulated the downstream target genes DUSP2 was dependent on miRNA122-5p, the expression of DUSP2 was analysed in the presence or absence of hsa-miR-122-5p inhibitor. We found that the suppressed expression of DUSP2 in the H-EVs treatment group could be reversed when miRNA hsa-miR-122-5p inhibitor was added (Fig. 6C, D). Concurrently, the increased autophagy level under H-EVs treatment was reduced by hsa-miR-122-5p inhibitor as indicated by expression levels of autophagy markers (Fig. 6E, G) and number of autophagosome (Fig. 6F). Similarly, H-EVs promotion of proliferation and migration of chondrocyte can be impeded by hsa-miR-122-5p inhibitor (Fig. 6H-J).

DUSP2 regulated by miR-122-5P involves chondrocyte autophagy through the MAPK pathway

To further clarify the regulatory role of DUSP2 on autophagy in chondrocyte regeneration, salubrinal, a DUSP2 inhibitor [24] was introduced. The non-toxic and effective concentration of salubrinal was identified to be 10nM by CCK8 test (Supplementary Fig. 2C). In the presence of salubrinal, the level of autophagy was increased regardless of IL-1 β treatment, as indicated by the expression of autophagy markers (Supplementary Fig. 6A, B, G), and the number of autophagosomes (Supplementary Fig. 6C). The level of autophagy decreased by hsa-miR-122-5p inhibitor could be rescued with the inclusion of DUSP2 inhibitor (Fig. 7A-D). Similarly, suppression of chondrocyte matrix formation (Fig. 7E, F), proliferation (Fig. 7G) and migration (Fig. 7H, I) imparted by hsa-miR-122-5p inhibitor was reversed by DUSP2 inhibitor. Taken together, these data indicate that miRNA122-5p in EVs participate in the autophagy regulation of chondrocytes by regulating downstream target genes DUSP2.

Through gene function enrichment analysis of the screened autophagy differential genes, we found that

GO terms include response to hormone, 14-3-3 protein binding, response to hypoxia, and response to oxygen levels (Fig. 7J). KEGG pathways suggested the PI3K-AKT pathway, FoxO pathway and MAPK pathway (Fig. 7K). Molecular interaction network composed of the top five molecules related to DUSP2 molecules include MAPK1, 3, 11 and 14 (Fig. 7L). Indeed, Western blot analysis shows that expression of p-ERK1/2 (MAPK3/1) and p-P38 (MAPK14) was upregulated in the presence of hsa-miR-122-5p inhibitor, which was reverted in the presence of salubrinal (Fig. 7M, N), suggesting that DUSP2 regulation by miR-122-5P in chondrocyte autophagy act through the MAPK pathway.

Discussion

Our study reveals that EVs released from hypoxia preconditioned human MSCs promote chondrocyte regeneration by regulating autophagy. We first assessed the therapeutic effect of hypoxic MSCs-produced EVs in a rat OA model. In addition, we investigated the impact of EVs on the regeneration of chondrocytes in vitro in both 2D and 3D culture platforms. MiRNA sequencing followed by study using specifically designed miRNA mimic and inhibitor further establish that miR122-5P from EVs promotes chondrocyte regeneration. By combining multiple database analysis, we identified DUSP2 as the downstream target of miR122-5P participating in the regulation of autophagy and validated DUSP2 involvement through inhibitor studies targeting both miR122-5P and DUSP2. Taken together, this study demonstrates that EVs released by MSCs under hypoxic conditions have a beneficial effect on chondrocyte regeneration. A novel mechanism for chondrocyte autophagy is mediated by miR122-5P and DUSP2 target molecules, providing new insights into OA treatments.

Constant advancement in the study of MSCs suggests unique therapeutic potential for cartilage repair, especially for OA [25]. EVs are the main active ingredients participating in MSCs paracrine activities, which have the advantages of easy collection, storage, stability, high bioavailability, and low immune exclusion [26]. Injection of EVs into the joint cavity can be used as cell-free therapy to repair cartilage damage [27]. Additionally, there is increasing evidence that different cultivation conditions may alter the therapeutic potential of MSCs [28]. MSCs cultured under physiological hypoxia condition, instead of the often used 21% O₂ had a beneficial effect on the

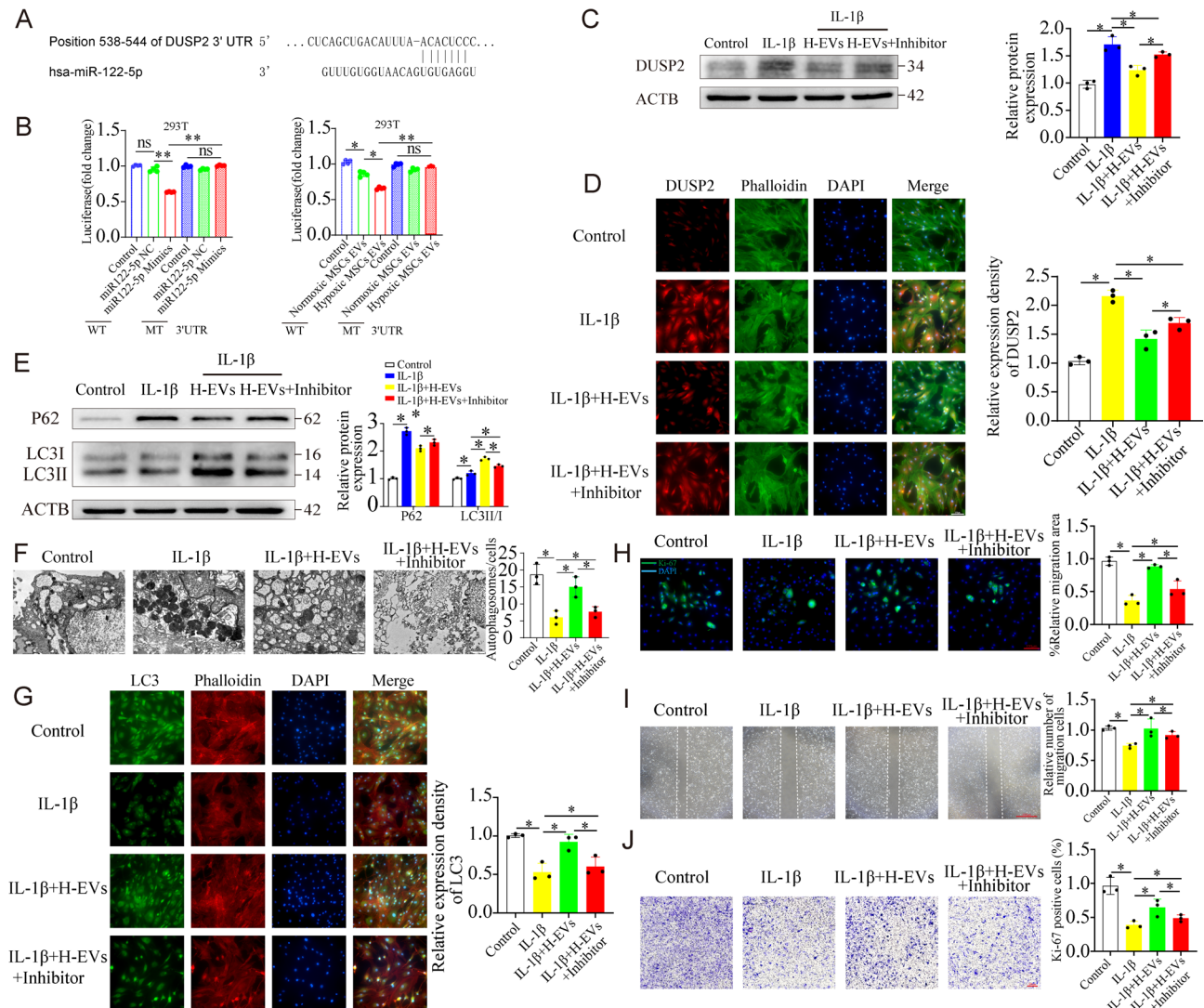


Fig. 6 EVs regulate chondrocyte autophagy dependent on miR-122-5p. **(A)** TargetScan analysis to predict the binding sequence between miR-122-5p and DUSP2. **(B)** Verification of direct binding between miR-122-5p mimics, or EVs, and DUSP2 by luciferase assay in 293T cells. **(C)** Western blot, and **(D)** immunofluorescence staining analysis of DUSP2 expression under H-EVs and miR-122-5p inhibitor treatment. **(E)** After adding H-EVs and miR-122-5p inhibitor, western-blot analysis of autophagy proteins expression after H-EVs and miR-122-5p inhibitor treatment. **(F)** TEM of autophagosomes in chondrocytes. **(G)** Immunofluorescence analysis of LC3. **(H)** Expression of Ki67 on the proliferation of chondrocytes. **(I)** Cell scratch assay, and **(J)** Trans-well migration analysis. Quantitative data represent mean \pm standard deviation, $n=5$; * denotes $p < 0.05$ and ** $p < 0.01$ relative to control group. Full-length blots are presented in Supplementary Fig. 7

biological nature of MSCs and its therapeutic potential [29]. Additionally, under the state of disease, hypoxia often occurs in tissue injury and inflammation. MSCs pre-treated in a hypoxic environment at 1 or 3% oxygen for 24–48 h generated exosomes with more effective regenerative activities in repairing cartilage [17, 30, 31]. In this study, we further study the effect of hypoxic MSC-generated EVs on OA development and decipher the role of EVs-derived microRNA, focusing on the regulation of autophagy.

MicroRNA serves as a crucial regulator of gene expression, which can bind to target mRNA, leading to RNA degradation or translation blockage [32]. MiRNAs play

a vital role in maintaining cellular homeostasis and regulating the pathophysiological processes of various diseases [33]. However, its own instability limits its application. Exosome-associated miRNAs are considered to be an effective and safe miRNA delivery vehicle and are beneficial for functionality, including in the treatment of OA diseases [34, 35].

In our study, miR-122-5p was found to be one of the highly upregulated miRNAs in H-EVs. It is a key microRNA involved in the regulation of numerous diseases, in particular in tumor cells. Researchers found that down-regulation of miR-122 could activate BCL9-mediated signaling pathways to predict the survival rate

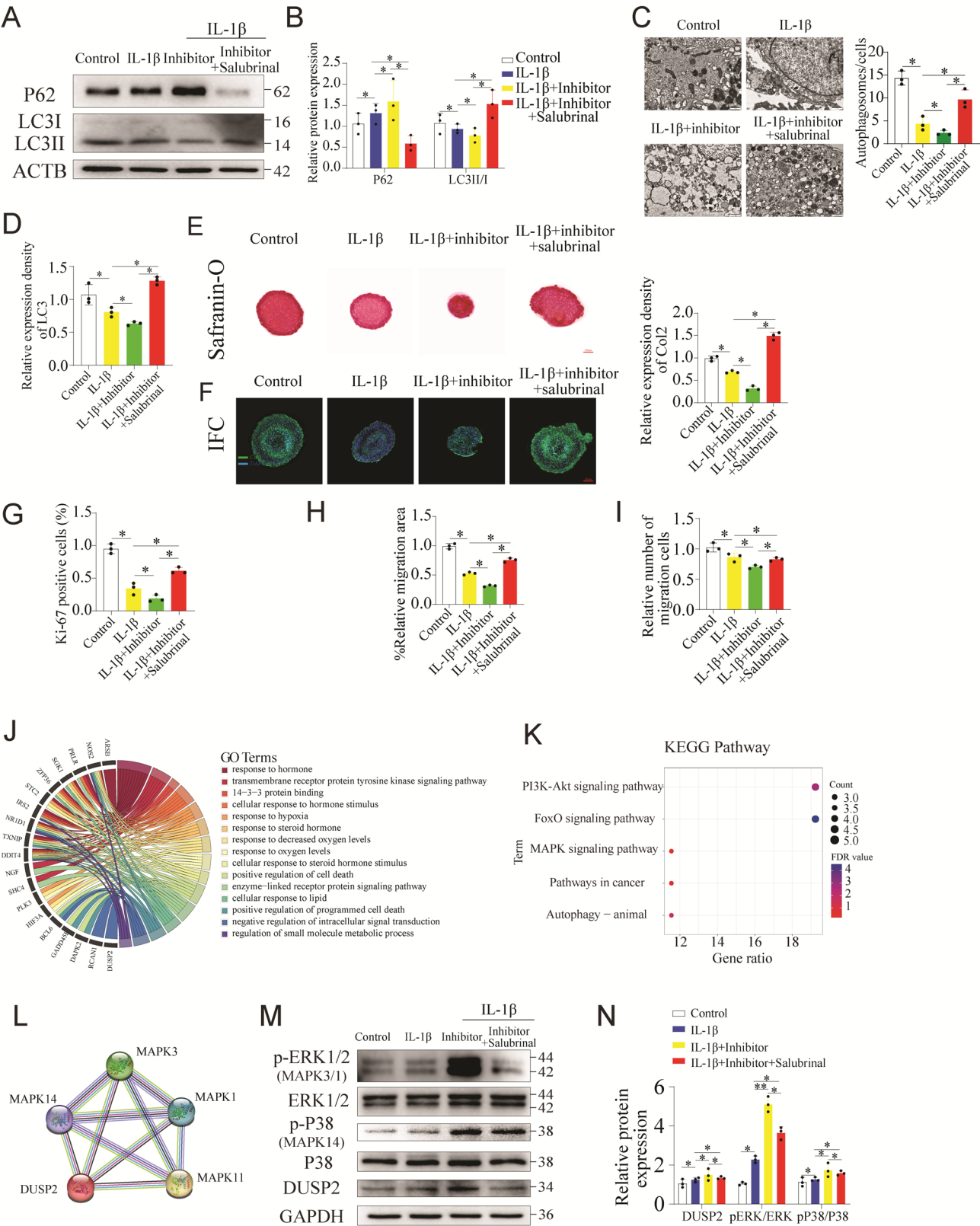


Fig. 7 (See legend on next page.)

(See figure on previous page.)

Fig. 7 miR-122-5P regulates chondrocyte autophagy dependent on DUSP2 and mediated the ERK1/2 and P38 pathways. **(A-B)** Expression of autophagy proteins with inhibition of miR-122-5P and DUSP 2. **(C)** TEM analysis of autophagosomes. **(D)** Immunofluorescence analysis of LC3. **(E-F)** Chondrocytes matrix proteins formation, **(G)** proliferation, and **(H-I)** migration under miR-122-5P and DUSP2 inhibition. **(J)** Circle diagram of GO enrichment analysis of autophagy-related differential genes in OA. **(K)** Bubble chart showing KEGG enrichment analysis. **(L)** The string database predicted that DUSP2 is involved in regulating downstream genes at the top5 genes. **(M)** Western-blot analysis of DUSP2 and MAPK protein expression under treatment by miR-122-5P inhibitor and DUSP2 inhibitor, salubrinal. **(N)** Quantitative data represent mean \pm standard deviation, $n=5$; * denotes $p < 0.05$ and ** $p < 0.01$ relative to sham group. Full-length blots are presented in Supplementary Fig. 7

of human liver cancer patients [36]. In pancreatic ductal adenocarcinoma disease, miR-122-5p was found to be insufficiently expressed in cancerous tumor tissues, and over-expression of miR-122-5p could inhibit cell proliferation, migration, invasion and EMT by down-regulating CCNG1 in pancreatic ductal adenocarcinoma [37]. MiRNA-122-5p also plays a regulatory role in the proliferation and migration of cardiac fibroblasts. MiRNA-122-5p is an important regulator of autophagy and apoptosis through the Apelin/AMPK/mTOR signaling pathway, which may serve as a therapeutic target for myocardial fibrosis and related diseases [38]. These studies indicate that miR-122-5p plays a significant role in regulating proliferation, migration, apoptosis, autophagy, and inflammation in various cell types. Increase expression of miR-122-5p was found in serum of OA and RA patients [39, 40]. We detected low levels of this miRNA in OA knee chondrocytes (Supplementary Fig. 9). Identification of miR-122-5p involvement in H-EVs regulated chondrocytes autophagy, proliferation, migration and matrix formation, ultimately leading to an inhibition of osteoarthritis progression is thus in accordance with the reported role of miR-122-5p.

We further linked miR-122-5p action to its downstream target, DUSP2. DUSP2 is a dual-specificity phosphatase, also known as activated cellular phosphatase 1 (PAC-1), capable of dephosphorylating dual threonine/tyrosine residues of substrates involved in multiple cell signal transduction pathways [41]. Numerous recent studies have highlighted the significant regulatory role of DUSP2 in cell proliferation, apoptosis, cancer, inflammation, and immune response [42–46]. However, the specific regulatory role of DUSP2 in the physiological function of chondrocytes in osteoarthritis remains under explored, especially in the regulation of autophagy. In the context of inflammatory arthritis research, Hamamura et al. have employed salubrinal, a DUSP2 inhibitors [24], to explore its effects on the expression of inflammatory cytokines in immune cells. The studies have demonstrated that silencing DUSP2 leads to a downregulation of IL-1 β levels, and salubrinal reduces the expression of inflammatory genes in macrophages, T lymphocytes, and mast cells, consequently alleviating inflammatory symptoms in mice [24]. Another study focused on intervertebral disc degenerative disease has shown that salubrinal can enhance the expression of COL2A1 and ACAN while reducing the level of up-regulated MMP-13 induced by

IL-17, effectively mitigating inflammation and delaying the degeneration of the intervertebral disc [47]. These findings are indicative of DUSP2 participation in degenerative cartilaginous tissues. In our study, abnormally high expression of DUSP2 was detected in the nuclei of chondrocytes, both in vitro in the IL-1 β -induced chondrocytes and in vivo OA cartilage tissues. We further found DUSP2 expression in chondrocytes extracted from knee cartilage tissues of OA patients (Supplementary Fig. 9). Employing salubrinal together with miR-122-5p inhibitor, we established for the first time the role of DUSP2 in chondrocytes autophagy, proliferation and migration. Interventions targeting DUSP2 contributed, to a certain extent, the improvement of osteoarthritis progression through autophagy.

As a member of the dual-specificity protein phosphatase subfamily, DUSP2 is predominantly expressed in the nucleus, and its expression varies significantly across different diseases and tissues. DUSP2 is well-known as a negative regulator of MAPK signaling, and inactivates its target kinases by dephosphorylating critical residues, including Erk1/2, p38, and JNK [48]. In vitro experiments have shown that DUSP2 preferentially dephosphorylates Erk1/2 and p38, but not JNK [49, 50]. In tendon injury disease, adult stem cell-derived large extracellular vesicles was found to exert detoxification effect through DUSP2 and DUSP3, which was responsible for regulating p38 MAPK signaling, polarizing M1 macrophages to M2 macrophages, resulting in pain and inflammation reduction in tendinopathy [51]. In the field of tumor research in the metastasis of pancreatic ductal adenocarcinoma (PDAC), overexpression of miR-361-3p promoted the migration and invasion of pancreatic cancer cells in vitro, and DUSP2 was shown as the direct target of miR-361-3p, which in turn caused ERK pathway inactivation, identifying the miR-361-3p/DUSP2/ERK axis as a novel EMT axis in PDAC [52]. Our study revealed that differential autophagy molecules in osteoarthritis are enriched in MAPK and autophagy pathways. We observed that DUSP2 negatively regulates the phosphorylation of ERK1/2 and P38, suggesting a miR-122-5p/DUSP2/MAPK axis in mediating the autophagy pathway in chondrocyte.

Conclusion

In summary, this study found that EVs derived from hypoxia-preconditioned human MSCs have the potential to reduce the development of OA by regulation of chondrocyte autophagy. We found that miR-122-5p from EVs regulates chondrocyte autophagy by modulating DUSP2 through MAPK pathway. These findings offer a novel perspective for promoting chondrocyte regeneration and ameliorating the progression of osteoarthritis, suggesting a potential avenue for treatment.

Supplementary Information

The online version contains supplementary material available at <https://doi.org/10.1186/s13287-025-04412-4>.

Supplementary Material 1

Supplementary Material 2

Supplementary Material 3

Supplementary Material 4

Supplementary Material 5

Supplementary Material 6

Supplementary Material 7

Acknowledgements

Majority of the study was performed in National University of Singapore. The authors are grateful to Lu Thong Beng and the Electron Microscopy Unit at the National University of Singapore for technical assistance with the electron microscopy. We thanks Asst Prof Barry Tan Wei Loong for providing the patients knee samples.

Author contributions

ZY, JHPH, YY acquired funding. HZ and ZY designed the studies. HZ, YW & YY performed in vivo study. HZ, YW, YY & VD, performed tissue analysis and curated data. HZ, YWJK, WZ & WMRL performed in vitro experiments and analysis. HZ & LL performed data mining and transcriptomic analysis. HZ, ZY & YY drafted and edited the manuscript. YY & JHPH reviewed the manuscript. All authors read and approved the final manuscript.

Funding

This work was supported by National Medical Research Council of Singapore (MOH-000371-00), Natural Science Foundation of Shanghai (No. 23ZR1451700) and Medical-Engineering Cross Project of Shanghai Jiao Tong University (YG2022QN076). HZ was supported by the China Scholarship Council (CSC NO. 202206920037).

Data availability

All data generated or analyzed during this study are included in this published articles and its supplementary information files.

Declarations

Ethics approval

All animal procedures were performed according to the guidelines of the Institutional Animal Care and Use Committee at National University of Singapore. Project Title: Cartilage tissue engineering with mesenchymal stem cells and extracellular vesicles from manipulated MSCs. Protocol number: R2020-0258. Approval date: 21/05/2020.

The access to human OA cartilage tissues was according to the guidelines of National Healthcare Group Domain Specific Review Board (NHG DSRB Ref: 2024–3392). Study title: Zonal chondrocytes for improved strategy of autologous chondrocyte implantation in cartilage repair. Approval date: 09/10/2024.

The original source for hMSC (Lonza; as stated in their Certificate of Analysis) and 293T/17 (ATCC, file:///C:/Users/dosyz/Downloads/CRL-11268%20Product%20Sheet%20-%2020293T_17%20[HEK%20293T_17].pdf) have confirmed that there was initial approval for collection of these human cell, and that the donors had signed informed consent. The information can be found on company website.

Consent for publication

Informed consent to participate in research study has been obtained.

Competing interests

The authors report no conflict of interest.

Received: 26 December 2024 / Accepted: 21 May 2025

Published online: 07 June 2025

References

1. Katz JN, Arant KR, Loeser RF. Diagnosis and treatment of hip and knee osteoarthritis: a review. *JAMA*. 2021;325(6):568–78.
2. van den Bosch MH. Osteoarthritis year in review 2020: biology. *Osteoarthritis Cartil*. 2021;29(2):143–50.
3. Abramoff B, Caldera FE. Osteoarthritis: pathology, diagnosis, and treatment options. *Med Clin*. 2020;104(2):293–311.
4. Molnar V, Matisić V, Kodvanj I, Bjelica R, Jeleč Ž, Hudetz D, et al. Cytokines and chemokines involved in osteoarthritis pathogenesis. *Int J Mol Sci*. 2021;22(17):9208.
5. Hussain S, Neilly D, Baliga S, Patil S, Meek R. Knee osteoarthritis: a review of management options. *Scott Med J*. 2016;61(1):7–16.
6. Tang Y, Li Y, Xin D, Chen L, Xiong Z, Yu X. Icarin alleviates osteoarthritis by regulating autophagy of chondrocytes by mediating PI3K/AKT/mTOR signaling. *Bioengineered*. 2021;12(1):2984–99.
7. Caramés B, Hasegawa A, Taniguchi N, Miyaki S, Blanco FJ, Lotz M. Autophagy activation by Rapamycin reduces severity of experimental osteoarthritis. *Ann Rheum Dis*. 2012;71(4):575–81.
8. Deng Z, Long D, Liu H, Xu Y, Xin R, Liao H, et al. tRNA-Derived fragment tRF-5009A regulates autophagy and degeneration of cartilage in osteoarthritis via targeting mTOR. *Oxid Med Cell Longev*. 2022;2022(1):5781660.
9. Yamamoto H, Zhang S, Mizushima N. Autophagy genes in biology and disease. *Nat Rev Genet*. 2023;24(6):382–400.
10. Glick D, Barth S, Macleod KF. Autophagy: cellular and molecular mechanisms. *J Pathol*. 2010;221(1):3–12.
11. Klionsky DJ, Petroni G, Amaravadi RK, Baehrecke EH, Ballabio A, Boya P, et al. Autophagy in major human diseases. *EMBO*. 2021;40(19):e108863.
12. Nguyen TH, Duong CM, Nguyen X-H, Than UTT. Mesenchymal stem cell-derived extracellular vesicles for osteoarthritis treatment: extracellular matrix protection, chondrocyte and osteocyte physiology, pain and inflammation management. *Cells*. 2021;10(11):2887.
13. Ni Z, Zhou S, Li S, Kuang L, Chen H, Luo X, et al. Exosomes: roles and therapeutic potential in osteoarthritis. *Bone Res*. 2020;8(1):25.
14. Wu J, Kuang L, Chen C, Yang J, Zeng W-N, Li T, et al. miR-100-5p-abundant exosomes derived from infrapatellar fat pad MSCs protect articular cartilage and ameliorate gait abnormalities via inhibition of mTOR in osteoarthritis. *Biomaterials*. 2019;206:87–100.
15. Wen C, Lin L, Zou R, Lin F, Liu Y. Mesenchymal stem cell-derived exosome mediated long non-coding RNA KLF3-AS1 represses autophagy and apoptosis of chondrocytes in osteoarthritis. *Cell Cycle*. 2022;21(3):289–303.
16. Lou C, Jiang H, Lin Z, Xia T, Wang W, Lin C, et al. MiR-146b-5p enriched bioinspired exosomes derived from fucoidan-directed induction mesenchymal stem cells protect chondrocytes in osteoarthritis by targeting TRAF6. *J Nanobiotechnol*. 2023;21(1):486.
17. Yang Y, Wu Y, Yang D, Neo SH, Kadir ND, Goh D, et al. Secretive derived from hypoxia preconditioned mesenchymal stem cells promote cartilage regeneration and mitigate joint inflammation via extracellular vesicles. *Bioactive Mater*. 2023;27:98–112.
18. Liu W, Rong Y, Wang J, Zhou Z, Ge X, Ji C, et al. Exosome-shuttled miR-216a-5p from hypoxic preconditioned mesenchymal stem cells repair traumatic spinal cord injury by shifting microglial M1/M2 polarization. *J Neuroinflammation*. 2020;17(1):47.

19. Zhang B, Tian X, Qu Z, Hao J, Zhang W. Hypoxia-Preconditioned extracellular vesicles from mesenchymal stem cells improve cartilage repair in osteoarthritis. *Membr (Basel)*. 2022;12(2).
20. Kohl M, Wiese S, Warscheid B. Cytoscape: software for visualization and analysis of biological networks. *Methods Mol Biol*. 2011;696:291–303.
21. Pham T, van der Heijde D, Altman R, Anderson J, Bellamy N, Hochberg M, et al. OMERACT-OARSI initiative: osteoarthritis research society international set of responder criteria for osteoarthritis clinical trials revisited. *Osteoarthr Cartil*. 2004;12(5):389–99.
22. Wang H, Zhang C, Zhang C, Wang Y, Zhai K, Tong Z. MicroRNA-122-5p regulates coagulation and inflammation through MASP1 and HO-1 genes. *Infect Genet Evol*. 2022;100:105268.
23. Li K-W, Wang S-H, Wei X, Hou Y-Z, Li Z-H. Mechanism of miR-122-5p regulating the activation of PI3K-Akt-mTOR signaling pathway on the cell proliferation and apoptosis of osteosarcoma cells through targeting TP53 gene. *Eur Rev Med Pharmacol Sci*. 2020;24(24).
24. Hamamura K, Nishimura A, Chen A, Takigawa S, Sudo A, Yokota H. Salubrinal acts as a Dusp2 inhibitor and suppresses inflammation in anti-collagen antibody-induced arthritis. *Cell Signal*. 2015;27(4):828–35.
25. You B, Zhou C, Yang Y. MSC-EVs alleviate osteoarthritis by regulating micro-environmental cells in the articular cavity and maintaining cartilage matrix homeostasis. *Ageing Res Rev*. 2023;85:101864.
26. Rilla K, Mustonen A-M, Arasu UT, Härkönen K, Matilainen J, Nieminen P. Extracellular vesicles are integral and functional components of the extracellular matrix. *Matrix Biol*. 2019;75:201–19.
27. Ren S, Wang C, Guo S. Review of the role of mesenchymal stem cells and exosomes derived from mesenchymal stem cells in the treatment of orthopedic disease. *Med Sci Monitor: Int Med J Experimental Clin Res*. 2022;28:e935937–11.
28. Kusuma GD, Carthew J, Lim R, Frith JE. Effect of the microenvironment on mesenchymal stem cell paracrine signaling: opportunities to engineer the therapeutic effect. *Stem Cells Dev*. 2017;26(9):617–31.
29. Yang Y, Lee EH, Yang Z. Hypoxia-conditioned mesenchymal stem cells in tissue regeneration application. *Tissue Eng Part B: Reviews*. 2022;28(5):966–77.
30. Shen K, Duan A, Cheng J, Yuan T, Zhou J, Song H, et al. Exosomes derived from hypoxia preconditioned mesenchymal stem cells laden in a silk hydrogel promote cartilage regeneration via the miR-205–5p/PTEN/AKT pathway. *Acta Biomater*. 2022;143:173–88.
31. Rong Y, Zhang J, Jiang D, Ji C, Liu W, Wang J, et al. Hypoxic pretreatment of small extracellular vesicles mediates cartilage repair in osteoarthritis by delivering miR-216a-5p. *Acta Biomater*. 2021;122:325–42.
32. Pager CT, Wehner KA, Fuchs G, Sarnow P. MicroRNA-mediated gene Silencing. *Prog Mol Biol Transl Sci*. 2009;90:187–210.
33. Hesse M, Arenz C. MicroRNA maturation and human disease. *MiRNA Maturation: Methods Protocols*. 2014:11–25.
34. Wang M, Yu F, Ding H, Wang Y, Li P, Wang K. Emerging function and clinical values of Exosomal MicroRNAs in cancer. *Mol therapy-Nucleic Acids*. 2019;16:791–804.
35. Ji Y, Xiong L, Zhang G, Xu M, Qiu W, Xiu C, et al. Synovial fluid exosome-derived miR-182-5p alleviates osteoarthritis by downregulating TNFAIP8 and promoting autophagy through LC3 signaling. *Int Immunopharmacol*. 2023;125:111177.
36. Luna JM, Barajas JM, Teng K-y, Sun H-L, Moore MJ, Rice CM, et al. Argonaute CLIP defines a deregulated miR-122-bound transcriptome that correlates with patient survival in human liver cancer. *Mol Cell*. 2017;67(3):400–10. e7.
37. Dai C, Zhang Y, Xu Z, Jin M. MicroRNA-122-5p inhibits cell proliferation, migration and invasion by targeting CCNG1 in pancreatic ductal adenocarcinoma. *Cancer Cell Int*. 2020;20:1–18.
38. Yang M, Song J-J, Yang X-C, Zhong G-Z, Zhong J-C. MiRNA-122-5p inhibitor abolishes angiotensin II-mediated loss of autophagy and promotion of apoptosis in rat cardioblasts by modulation of the apelin-AMPK-mTOR signaling. *Vitro Cell Dev Biology-Animal*. 2022;58(2):136–48.
39. Kong R, Gao J, Si Y, Zhao D. Combination of Circulating miR-19b-3p, miR-122-5p and miR-486-5p expressions correlates with risk and disease severity of knee osteoarthritis. *Am J Translational Res*. 2017;9(6):2852.
40. Yadav R, Srivastava RN, Kumar D, Sharma A, Srivastava SR, Pant S et al. Role of serum Micro-RNA-122-5p expression as a circulatory biomarker in people having both knee osteoarthritis and osteoporosis: A Case-Control study. *Cureus*. 2024;16(5).
41. Jeffrey KL, Camps M, Rommel C, Mackay CR. Targeting dual-specificity phosphatases: manipulating MAP kinase signalling and immune responses. *Nat Rev Drug Discovery*. 2007;6(5):391–403.
42. Rohan PJ, Davis P, Moskaluk CA, Kearns M, Kruttsch H, Siebenlist U, et al. PAC-1: a mitogen-induced nuclear protein tyrosine phosphatase. *Science*. 1993;259(5102):1763–6.
43. Wei W, Jiao Y, Postlethwaite A, Stuart J, Wang Y, Sun D, et al. Dual-specificity phosphatases 2: surprising positive effect at the molecular level and a potential biomarker of diseases. *Genes Immun*. 2013;14(1):1–6.
44. Lin S-C, Chien C-W, Lee J-C, Yeh Y-C, Hsu K-F, Lai Y-Y, et al. Suppression of dual-specificity phosphatase-2 by hypoxia increases chemoresistance and malignancy in human cancer cells. *J Clin Invest*. 2011;121(5):1905–16.
45. Yin Y, Liu Y-X, Jin YJ, Hall EJ, Barrett JC. PAC1 phosphatase is a transcription target of p53 in signalling apoptosis and growth suppression. *Nature*. 2003;422(6931):527–31.
46. Morente V, Pérez-Sen R, Ortega F, Huerta-Cepas J, Delicado EG, Miras-Portugal MT. Neuroprotection elicited by P2Y13 receptors against genotoxic stress by inducing DUSP2 expression and MAPK signaling recovery. *Biochimica et biophysica acta (BBA)-Molecular. Cell Res*. 2014;1843(9):1886–98.
47. Yao Z, Nie L, Zhao Y, Zhang Y, Liu Y, Li J, et al. Salubrinal suppresses IL-17-induced upregulation of MMP-13 and extracellular matrix degradation through the NF- κ B pathway in human nucleus pulposus cells. *Inflammation*. 2016;39:1997–2007.
48. Owens D, Keyse S. Differential regulation of MAP kinase signalling by dual-specificity protein phosphatases. *Oncogene*. 2007;26(22):3203–13.
49. Chu Y, Solski PA, Khosravi-Far R, Der CJ, Kelly K. The Mitogen-activated protein kinase phosphatases PAC1, MKP-1, and MKP-2 have unique substrate specificities and reduced activity in vivo toward the ERK2 Sevenmaker mutation (*). *J Biol Chem*. 1996;271(11):6497–501.
50. Ward Y, Gupta S, Jensen P, Wartmann M, Davis RJ, Kelly K. Control of MAP kinase activation by the mitogen-induced threonine/tyrosine phosphatase PAC1. *Nature*. 1994;367(6464):651–4.
51. Ye T, Chen Z, Zhang J, Luo L, Gao R, Gong L, et al. Large extracellular vesicles secreted by human iPSC-derived MSCs ameliorate tendinopathy via regulating macrophage heterogeneity. *Bioactive Mater*. 2023;21:194–208.
52. Hu J, Li L, Chen H, Zhang G, Liu H, Kong R, et al. MiR-361-3p regulates ERK1/2-induced EMT via DUSP2 mRNA degradation in pancreatic ductal adenocarcinoma. *Cell Death Dis*. 2018;9(8):807.

Publisher's note

Springer Nature remains neutral with regard to jurisdictional claims in published maps and institutional affiliations.